Hydration study of slag-blended cement based on thermodynamic considerations

Yogarajah Elakneswaran [1]*, Eiji Owaki [2], Shigeyoshi Miyahara [2], Masataka Ogino [2], Tsuyoshi Maruya [2], Toyoharu Nawa [1]

[1]Division of Sustainable Resources Engineering
Faculty of Engineering
Hokkaido University
Kita 13, Nishi 8, Kita-ku, Sapporo,
060-8628, Japan

[2]Civil Structure and Material Research Section,
Civil Engineering Research Institute
Technology Centre, Taisei Corporation
344-1, Nase-cho, Totsuka-ku, Yokohama
245-0051, Japan

* Corresponding author
E-mail: elakneswaran@eng.hokudai.ac.jp
Tel: +81-11-706-6918, Fax: +81-11-706-6918

Abstract

Thermodynamic calculations, using the geochemical code PHREEQC coupled with empirical equations for kinetics of cement hydration and slag reaction, were carried out to predict the compositions of the hydrate assemblage and pore solutions of hydrating Portland cement and

cement blended with slag and the blended cement containing limestone. The predicted compositions of hydration products and element concentrations in pore solutions compared well with experimental data reported in literature. The calculation results showed the varying Ca/Si and Al/Si ratios of calcium aluminosilicate hydrate (C-A-S-H)* in the hydration products due to hydration and slag addition. Limitations on the equation for reaction of slag and the importance of a C-A-S-H solid solution model in prediction of hydration products are discussed.

Keywords: Thermodynamic Calculations; Slag-blended Cement; Hydration Products; Pore Solution; PHREEQC

1. INTRODUCTION

A partial replacement of Portland cement (PC) by supplementary cementitious materials (SCMs) or innovative low-carbon cement-based materials can substantially reduce CO_2 emissions associated with PC production [1]. Several studies have focused on developing SCMs from a variety of waste and by-product materials, in addition to common SCMs such as fly ash, ground granulated blast-furnace slag, and silica fume [2]. Further, novel cement systems/concrete are being developed through alkaline activation of aluminosilicates or innovative uses of waste materials [3]. Some of these novel cements are in use on a limited scale in some parts of the world; however, their short- and long-term performance as compared to conventional PC needs to be established for their large-scale application [1]. More investigation on the properties and performance of SCMs or novel cements is necessary for their successful usage as partial or complete replacement of PC in concrete.

Knowledge of hydrating cement and the cementitious behaviour and pozzolanic characteristics of

* Cement chemistry shorthand notations: A = Al_2O_3, C = CaO, S = SiO_2, and H = H_2O

SCMs are important for better understanding of the properties and performance of the materials in concrete. It is also essential in terms of materials selection for concrete and for predicting properties and the durability and structural performance of concrete. The properties of hydrated PC and blended cement can be determined by laboratory experiments. However, it is difficult to depend entirely on experimental methods to determine the properties owing to the variety of SCMs used and the time it takes to perform these experiments. On the other hand, thermodynamic or mathematical models significantly reduce the reliance on laboratory experiments and help to predict hydration processes and materials properties.

Thermodynamic models in cementitious systems would make it possible to predict the composition of the hydrate assemblage and the aqueous phase composition based on information about the starting materials. Rothstein [4] studied the saturation indexes of solid phases in hydrating PC during the first 28 days of hydration using thermodynamic analysis of the element concentrations and compared the calculated saturation indexes with the supersaturation of phases found in previous work. Lothenbach and associates [5-12] made significant contributions to the thermodynamic calculations for cementitious materials to better understand cement hydration processes. Their work facilitated prediction of the composition of solid and liquid phases during hydration as a function of hydration time and simulation of the phase changes in cementitious materials in contact with ionic solutions. A thermodynamic model developed using the Gibbs free energy minimisation program GEMS-PSI (available at http://gems.web.psi.ch/) coupled with kinetic equations for the dissolution of clinker minerals successfully predicted the solid-phase assemblage and pore solution composition of hydrated PC [7] and PC-containing limestone [7 and 9]. The model was extended to allow calculations in the temperature range of 0–100 °C [10]; it was also applied to various cements [8] and mineral admixtures [5 and 12]. In addition to thermodynamic models, several hydration models in cementitious materials have been proposed to simulate the hydration reaction of cement and slag and also to predict the evolution of hydration products [13-14]. It is recognised that a

partial or complete replacement of PC with slag reduces the Ca/Si ratio of calcium silicate hydrate (C-S-H) and also forms calcium aluminosilicate hydrate (C-A-S-H) [2, and 15-16]. The incorporation of aluminium in C-S-H of PC has also been reported in previous studies [2 and16]. However, details of these aspects have not yet been taken into account in existing models for predicting the composition of the hydrate assemblage and pore solution chemistry. A model that includes Al incorporation and various Ca/Si ratios of C-S-H is thus important for better prediction of the solid products and aqueous phase compositions formed in PC and slag-blended systems.

In this study, chemical thermodynamic calculations were carried out to predict the solid-phase assemblages and pore solution composition of hydrating PC and slag as a function of hydration time. An integrated model that coupled PHREEQC [17-18] with empirical expressions for dissolution of clinker minerals and reactions of slag was developed, in which, the reactions among solids, aqueous solutions, and solid solutions were considered simultaneously at each hydration time step. Various calculation features built into PHREEQC including phase-equilibrium, speciation, and solid solutions, allowed the performance of a variety of geochemical calculations at higher ionic strengths as well, using an incorporated Pitzer model [19]. A solid solution that consists of various C-S-H and C-A-S-H gels as end-members was considered to account for the changing Ca/Si ratio and aluminium uptake in the gels [15 and 20]. The results of thermodynamic calculations in terms of solid-phase composition and concentration of elements in the pore solution were compared with the experimental data in literature for hydrating PC, cement blended with slag, and blended cement containing limestone.

2. MODEL DESCRIPTION

2.1. Thermodynamic model

In this study, a phase-equilibrium module in PHREEQC was employed to carry out thermodynamic

equilibrium calculations [17-18]. When a pure phase is no longer in equilibrium with a solution, it will dissolve or precipitate. The equilibrium reactions are expressed by the mass-action equation as

$$K_p = \prod_i \left(\gamma_i c_i\right)^{n_{i,p}} \quad (1)$$

where K_p is the thermodynamic equilibrium constant for phase p, γ_i is the activity coefficient of ion i (−), c_i is the concentration of ion i (mol/L), and $n_{i,p}$ is the stoichiometric coefficient of ion i in phase p (−). The thermodynamic equilibrium constant, K_p, at a given temperature T (K) can be expressed as

$$K_p = \exp\left(-\frac{\Delta_r G_T^0}{RT}\right) \quad (2)$$

where $\Delta_r G_T{}^0$ is the standard Gibbs energy of reaction at temperature T and R is the universal gas constant (8.31451 J/(mol K)). The standard Gibbs energy of reaction is expressed as

$$\Delta_r G_T^0 = \sum \Delta_f G_{T,products}^0 - \sum \Delta_f G_{T,reactants}^0 \quad (3)$$

where $\Delta_f G_T{}^0$ is the Gibbs free energy of formation for a species at a given temperature T. The equilibrium constant ($logK_p$) and the standard heats of reaction ($\Delta_r H^0$), which is used in the Van't Hoff equation (Appelo and Postma 2009) to determine temperature dependence of the equilibrium constant, for the dissolution reactions of phases used in the simulation are tabulated in **Table 1**. The name of the phase (defined by dissolution reaction, $logK_p$, and $\Delta_r H^0$, as given in **Table 1**), the specified saturation index (which has a value of zero for equilibrium), and the amount of the phase were the input parameters for the phase-equilibrium module in PHREEQC.

129 **Table 1** Thermodynamic properties of the phases at 25˚C used in the calculation**s** [10, 15, and 18]

Phase	Reactions	logK_p	$\triangle_r H^0$	Ref.
Anhydrite	$CaSO_4 \leftrightarrow Ca^{2+} + SO_4^{2-}$	-4.36	-1.71	[18]
Brucite	$Mg(OH)_2 + 2H^+ \leftrightarrow Mg^{2+} + 2H_2O$	17.07	-115.66	[10]
C_3AH_6	$Ca_3Al_2(OH)_{12} + 12H^+ \leftrightarrow 3Ca^{2+} + 2Al^{3+} + 12H_2O$	82.22	-595.76	[10]
C_3FH_6	$Ca_3Fe_2(OH)_{12} + 12H^+ \leftrightarrow 3Ca^{2+} + 2Fe^{3+} + 12H_2O$	73.65	-516.96	[10]
Calcite	$CaCO_3 \leftrightarrow Ca^{2+} + CO_3^{2-}$	-8.48	-2.297	[18]
CASH_5CA	$(CaO)_{1.25}(Al_2O_3)_{0.125}(SiO_2):1.625H_2O + 3.25H^+ \leftrightarrow 1.25Ca^{2+} + 0.25Al^{3+} + H_4SiO_4 + 1.25H_2O$	22.00	-141.58	[15]
CASH_INFCA	$(CaO)(Al_2O_3)_{0.15625}(SiO_2)_{1.1875}:1.65625H_2O + 2.9375H^+ \leftrightarrow Ca^{2+} + 0.3125Al^{3+} + 1.1875H_4SiO_4 + 0.75H_2O$	16.60	-110.67	[15]
CSH_T2C	$(CaO)_{1.5}(SiO_2):2.5H_2O + 3H^+ \leftrightarrow 1.5Ca^{2+} + H_4SiO_4 + 2H_2O$	25.88	-127.10	[15]
CSH_T5C	$(CaO)_{1.25}(SiO_2)_{1.25}:2.5H_2O + 2.5H^+ \leftrightarrow 1.25Ca^{2+} + 1.25H_4SiO_4 + 1.25H_2O$	18.74	-83.46	[15]
CSH_Jen	$(CaO)_{1.667}(SiO_2):2.1H_2O + 3.334H^+ \leftrightarrow 1.667Ca^{2+} + H_4SiO_4 + 1.767H_2O$	29.60	-148.44	[10]
CSH_TobH	$(CaO)(SiO_2)_{1.5}:2.5H_2O + 2H^+ \leftrightarrow Ca^{2+} + 1.5H_4SiO_4 + 0.5H_2O$	13.18	-47.83	[15]
Ettringite	$Ca_6Al_2(SO_4)_3(OH)_{12}:26H_2O + 12H^+ \leftrightarrow 6Ca^{2+} + 2Al^{3+} + 3SO_4^{2-} + 38H_2O$	57.73	-389.36	[10]
Gypsum	$CaSO_4:2H_2O \leftrightarrow Ca^{2+} + SO_4^{2-} + 2\ H_2O$	-4.58	-0.109	[18]
Hemicarboaluminate	$Ca_4Al_2(CO_3)_{0.5}(OH)_{13}:5.5H_2O + 13H^+ \leftrightarrow 4Ca^{2+} + 2Al^{3+} + 0.5CO_3^{2-} + 18.5H_2O$	87.88	-604.27	[10]
Hydrotalcite	$Mg_4Al_2(OH)_{14}:3H_2O + 14H^+ \leftrightarrow 2Al^{3+} + 4Mg^{2+} + 17H_2O$	75.97	-607.91	[10]
Monocarboaluminate	$Ca_4Al_2(CO_3)(OH)_{12}:5H_2O + 12H^+ \leftrightarrow 4Ca^{2+} + 2Al^{3+} + CO_3^{2-} + 17H_2O$	71.54	-533.14	[10]
Monosulfoaluminate	$Ca_4Al_2(SO_4)(OH)_{12}:6H_2O + 12H^+ \leftrightarrow 4Ca^{2+} + 2Al^{3+} + SO_4^{2-} + 18H_2O$	73.68	-553.08	[10]
Portlandite	$Ca(OH)_2 + 2H^+ \leftrightarrow Ca^{2+} + 2H_2O$	22.79	-129.66	[10]
Stratlingite	$Ca_2Al_2SiO_2(OH)_{10}:3H_2O + 10H^+ \leftrightarrow 2Ca^{2+} + 2Al^{3+} + H_4SiO_4 + 11H_2O$	51.42	-408.12	[10]

130

131 **2.2. Cement hydration model**

In this study, the cement hydration model proposed by Parrot and Killoh [21] was used to estimate the hydration degree of each cement clinker mineral as a function of time. The model is described in detail elsewhere [7, 9, and 21]; the main equations are briefly described here. Parrot and Killoh [21] derived a set of empirical equations to describe the hydration rate, R_t^m, of an individual clinker mineral m at time t (m = C_3S, C_2S, C_3A, C_4AF):

Nucleation and growth

$$R_{t,1}^m = \frac{K_1}{N_1}\left[1-\alpha_t^m\right]\left\{-\ln\left(1-\alpha_t^m\right)\right\}^{(1-N_1)} \quad (4)$$

Diffusion

$$R_{t,2}^m = \frac{K_2\left(1-\alpha_t^m\right)^{2/3}}{1-\left(1-\alpha_t^m\right)^{1/3}} \quad (5)$$

Hydration shell formation

$$R_{t,3}^m = K_3\left(1-\alpha_t^m\right)^{N_3} \quad (6)$$

The associated empirical parameters in the equations are tabulated in **Table 2** as reported by Lothenbach *et al*. [9-10]. The minimum among above the rates ($R_{t,1}^m, R_{t,2}^m, R_{t,3}^m$) is considered to be the controlling rate. The hydration degree of clinker mineral m at the time t, α_t^m, is calculated from the hydration degree of the mineral at the previous time step (α_{t-1}^m), the time interval (Δ_t), and hydration rate of the clinker mineral at the previous time step (R_{t-1}^m) as

$$\alpha_t^m = \alpha_{t-1}^m + \Delta t \cdot \min\left(R_{t-1,1}^m, R_{t-1,2}^m, R_{t-1,3}^m\right) \cdot \beta_{w/c} \cdot \lambda_{RH} \cdot \frac{A}{A_0} \cdot \exp\left[\frac{E_a^m}{R}\left(\frac{1}{T_0} - \frac{1}{T}\right)\right] \quad (7)$$

where,

$$\beta_{w/c} = \left[1 + 3.333 \times \left(H^m \times w/c - \alpha_{t-1}\right)\right]^4 \quad \text{if} \quad \alpha_t > H^m \times w/c$$

$$\beta_{w/c} = 1 \quad \text{if} \quad \alpha_t \leq H^m \times w/c \quad (8)$$

$$\lambda_{RH} = \left(\frac{RH - 0.55}{0.45}\right)^4 \quad (9)$$

where H^m is the critical degree of the clinker mineral m, w/c is the water to cement ratio, α_{t-1} is the total hydration degree of cement at the previous time step, A is the Blaine surface area of cement (m^2/kg), A^0 is the reference surface area of cement (385 m^2/kg), E_a^m is the apparent activation energy of clinker mineral m (J/mol), T_0 is the reference temperature (293.15 K), and RH is the relative humidity. The adapted values for H^m and E_a^m are based on the work by Lothenbach *et al*. [9-10], given in **Table 2**.

The total hydration degree of cement, α_t, relative to the total clinker content at time t is expressed by

$$\alpha_t = \frac{f^{C_3S}\alpha_t^{C_3S} + f^{C_2S}\alpha_t^{C_2S} + f^{C_3A}\alpha_t^{C_3A} + f^{C_4AF}\alpha_t^{C_4AF}}{f^{C_3S} + f^{C_2S} + f^{C_3A} + f^{C_4AF}} \quad (10)$$

where f^m is the relative mass fraction of the cement clicker mineral m.

Table 2 Parameters adapted to calculate the hydration degree of the clinker minerals as a function of time [9-10]

	C_3S	C_2S	C_3A	C_4AF
K_1	1.5	0.5	1	0.37

N_1	0.7	1	0.85	0.7
K_2	0.05	0.006	0.04	0.015
K_3	1.1	0.2	1	0.4
N_3	3.3	5	3.2	3.7
H	1.8	1.35	1.60	1.45
E_a (J/mol)	41570	20785	54040	34087

3. SIMULATION RESULTS AND VERIFICATIONS

3.1. Ordinary Portland cement system

3.1.1. Modelling approach

PHREEQC was coupled (using the IPhreeqc module [22]) with Excel® to carry out thermodynamic calculations in each time step. PHREEQC performs speciation and batch-reaction calculations to calculate the solution composition and the kind and amount of precipitated phases based on a thermodynamic dataset and input parameters. The calculations on the dissolution rate of clinker minerals were carried out in Excel® and the necessary data were transferred to PHREEQC as input parameters. The thermodynamic properties for various phases and minerals found in cement system were collected from CEMDATA07 [10] and others [15], and the data were converted into a format suitable for PHREEQC; the data are given in **Table 1**. The converted data, together with the PHREEQC default thermodynamic database [18], were used in in this study for every calculation. The following assumptions were considered to determine the compositions of the solid phases and pore solutions using the coupled model:

- ✧ Free lime and alkali sulphates are dissolved completely as the cement comes into contact with water. Ca, O as OH, Na, K, and S are released into the pore solution.
- ✧ Cement clinker minerals are dissolved according to Eqs. (4) – (9) as a function of time and release Ca, Si, O as OH, Al, and Fe into the pore solution.
- ✧ Na_2O and K_2O, which are present as minor components in the clinker minerals, and total MgO are dissolved by the total hydration degree of the cement and release Na, K, Mg, and O as OH

into the pore solution.

- ✧ Gypsum and calcite react continuously to reach equilibrium with the pore solution.
- ✧ The elements released into the pore solution form minerals and phases through thermodynamic equilibrium.
- ✧ An ideal solid solution of six end-members (CASH_5CA, CASH_INFCA, CSH_T2C, CSH_T5C, CSH_Jen, and CSH_TobH, as given in **Table 1**) is assumed for C-S-H and C-A-S-H.

The alkalis are released from readily soluble alkalis sulphates and the dissolution of the clinker minerals. It is well known that a part of the released alkalis are taken up by C-A-S-H gel, and a distribution ratio (Rd_{Na}) of 0.45 mL/g is used for Na^+ uptake by C-A-S-H gel while the distribution ratio of K^+ (Rd_K) is expressed as follows [23]:

$$Rd_K = 0.20C_K^{-0.76} \quad (11)$$

where C_K is the concentration of K^+.

3.1.2. Simulation results and experimental data verification

The predicted phase changes as a function of time for Ordinary Portland Cement (OPC) paste (using the input parameters given in **Table 3**) are shown in **Fig. 1**(A). The model predicts the complete dissolution of the available gypsum in the cement within the first 7 h of hydration and the gradual increase in the amount of C-A-S-H end-members and portlandite with time. The presence of CSH_TobH and CASH_INFCA end-members in C-A-S-H solid solution is negligible. Magnesium present in the cement is predicted as brucite at an early age and then converted to hydrotalcite after 0.5 days of hydration. The model also calculates the continuous dissolution of

calcite present in the cement to form monocarboaluminate, and some monocarboaluminate transforms to hemicarboaluminate. The predicted phases in the hydrated OPC (after 7 days or longer of hydration time) include C-A-S-H gel solid solution, portlandite, ettringite, hydrotalcite, and AFm phases such as monocarboaluminate and hemicarboaluminate, in addition to un-hydrated clinker minerals. The chemical composition data for end-members of the C-A-S-H gel solid solution are used to predict the Ca/Si and Al/Si ratios of the gel (**Fig. 1**(B)). The predicted ratios of hydrating OPC are $1.48 \leq Ca/Si \leq 1.53$ and $0.003 \leq Al/Si \leq 0.049$.

Table 3 Chemical composition and Blaine surface area of OPC and mixing conditions as input to the model, adapted from ref. [9]

Phase composition (g/100 g)		*Minor components in the clinker phases*	
-Alite	66.5	-Na_2O	0.33
-Belite	10.3	-K_2O	0.06
-Aluminate	7.5	-MgO	1.8*
-Ferrite	8.5	*Mixing conditions*	
-CaO_Free	0.93	-w/c	0.4
-Calcite	0.6	-Temp ($^{\circ}$C)	20
-Gypsum	3.1	-RH (%)	1.0
-Na_2SO_4	0.21		
-K_2SO_4	1.33	Blaine surface area (m^2/kg)	413

* Total MgO

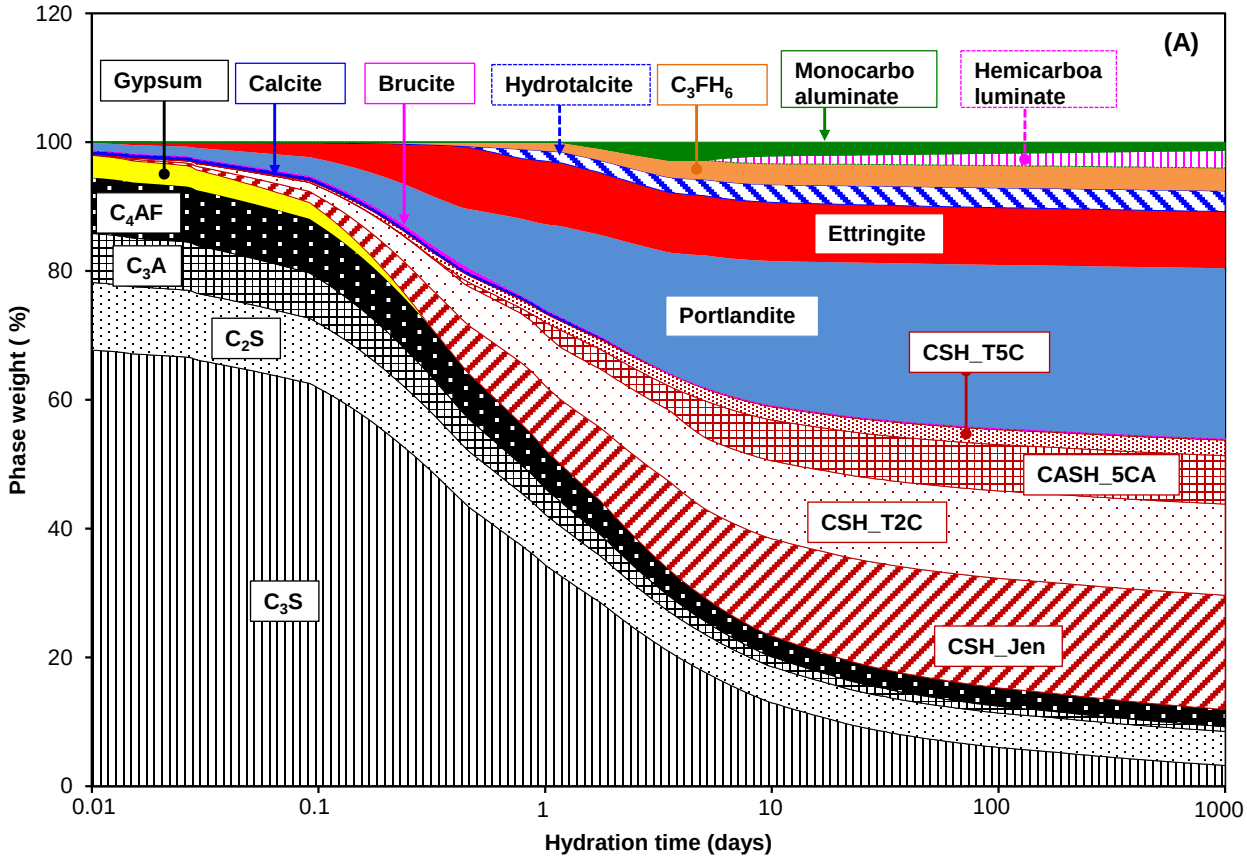

238

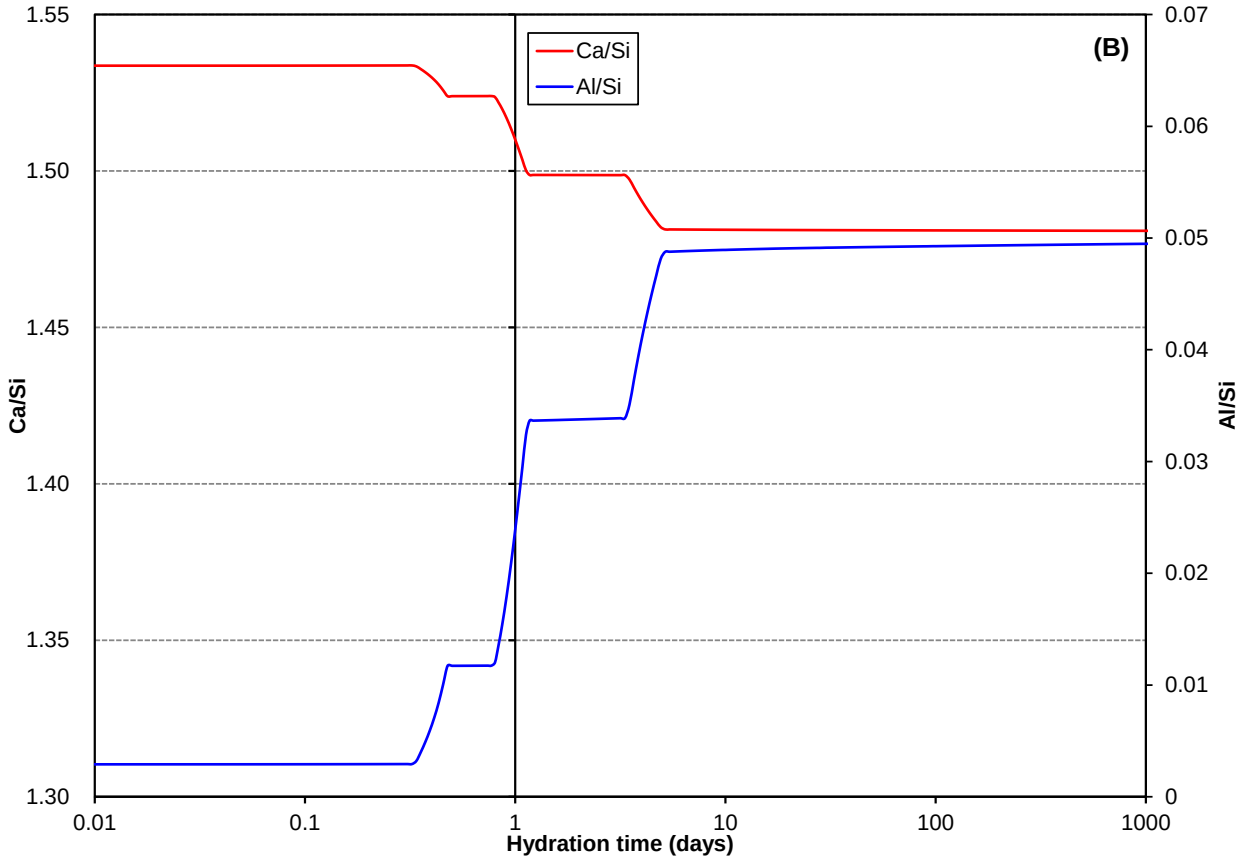

239

240 **Fig. 1.** Simulated phase (A), Ca/Si and Al/Si ratios of C-A-S-H (B) changes as a function of

241 hydration time for OPC

The simulated hydration products of OPC paste for the input parameters listed in **Table 3** were compared with the experimental data available in the literature [9], shown in **Fig. 2**. As reported by Matschei [24] and validated by Lothenbach *et al*. [9], the AFm phases determined by XRD (X-ray Diffraction) are certainly underestimated owing to their poor crystalline structure, relatively low amount, and lack of data concerning the structure. Therefore, the total amorphous content (C-S-H + amorphous AFm) from XRD measurement was compared with the summation of C-S-H and monosulfoaluminate from the current simulation. As illustrated in **Fig. 2**, the predicted hydration products of OPC are consistent with both the qualitative and quantitative experimental results as a function of hydration time.

The ionic concentration in the pore solution was calculated based on the release and uptake of alkalis as well as the thermodynamic equilibrium between the phases and the pore solution. The comparison of computed elements concentration in the pore solution of hydrating OPC (for the input parameters of **Table 3**) with experimentally determined ones [9] are shown in **Fig. 3**. The model predicts reasonably well the changes of major elements such as Na, K, OH, Ca, S, Al, and Si with hydration time, but the model cannot predict the presence of other elements such as Li, Sr, Ba, Cr, and Mo, even though they can be detected in the experiments. The simulated concentration of ions in pore solution is compared with another experimental data [25] to give further validation to the proposed model. The simulated concentration of Na, K, and Ca elements and pH of pore solution are compared with experimental values of hydrating OPC with varying w/c ratios in **Fig. 4**. It can be seen that the concentration of ions are predicted well though some discrepancies are observed for pH at 1 and 3 days.

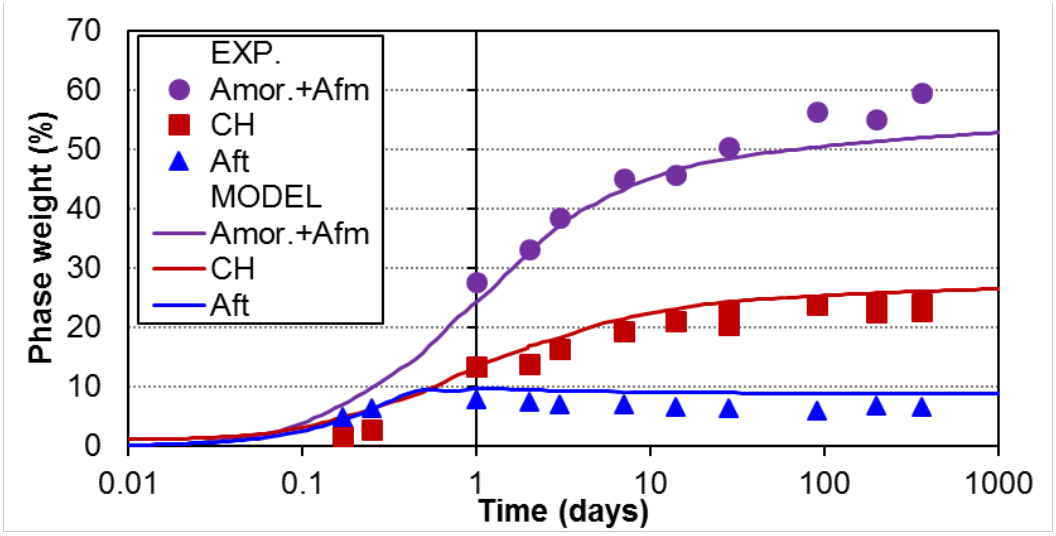

Fig. 2. Comparison of simulated portlandite, ettringite, and amorphous + Afm changes with experimental data [9] for hydrating OPC

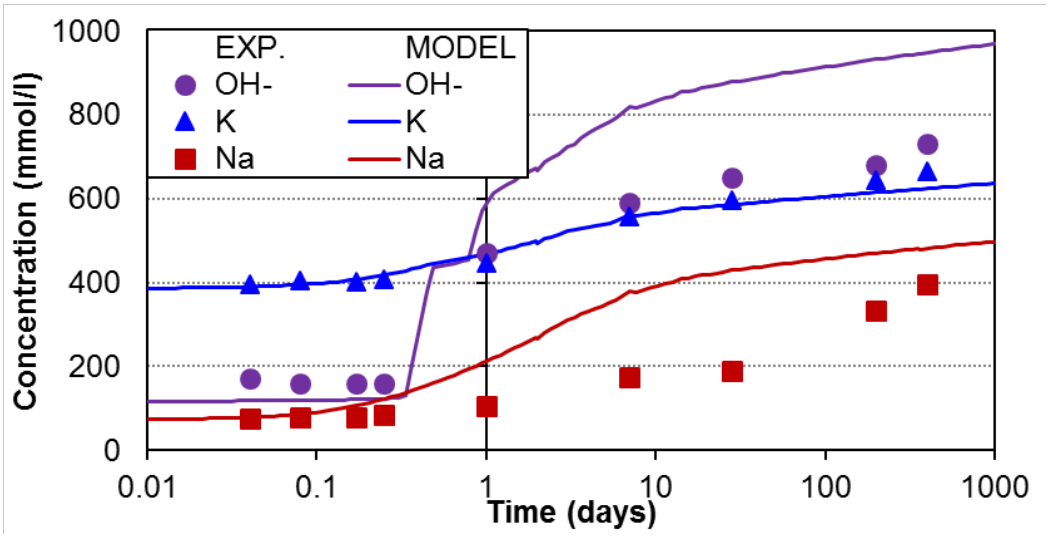

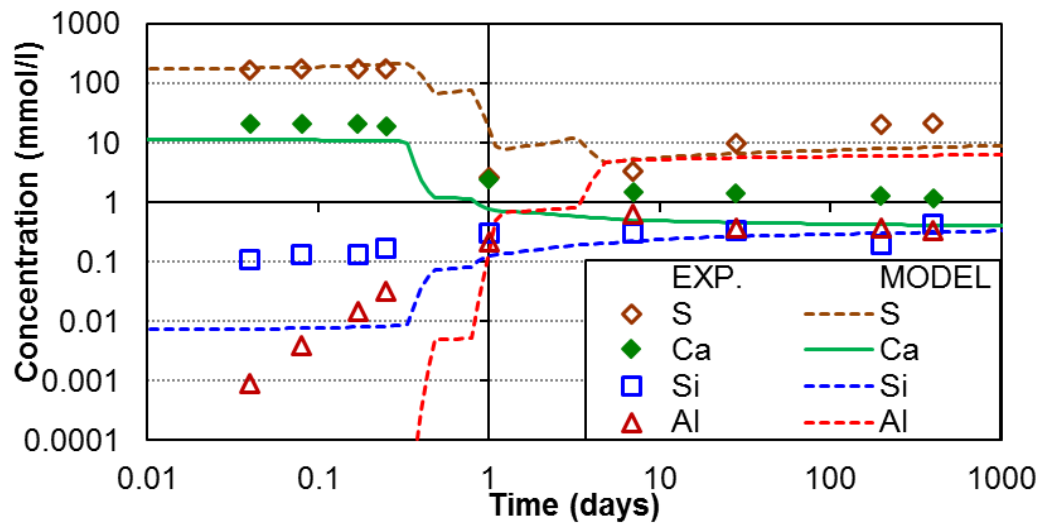

Fig. 3. Comparison of simulated pore solution concentration changes with experimental data [9] for hydrating OPC

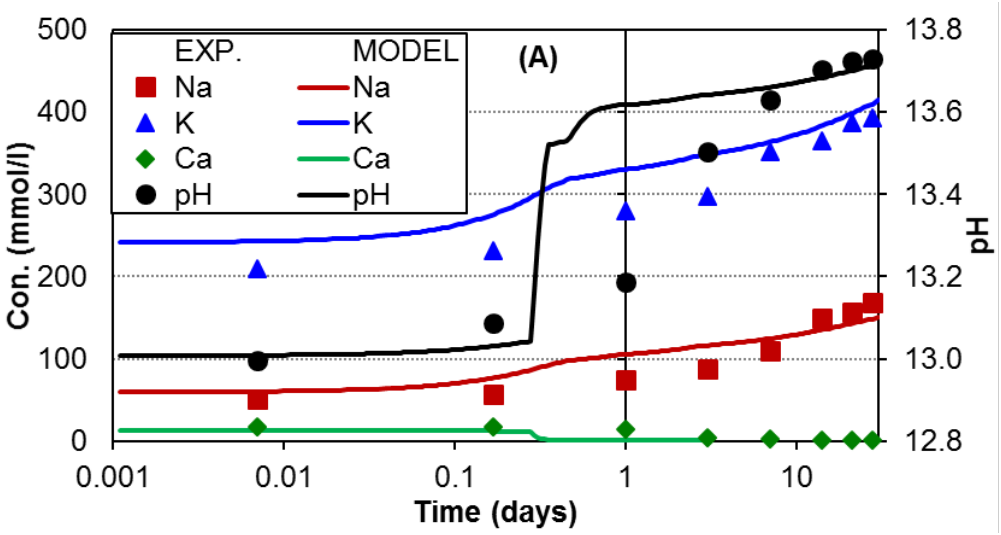

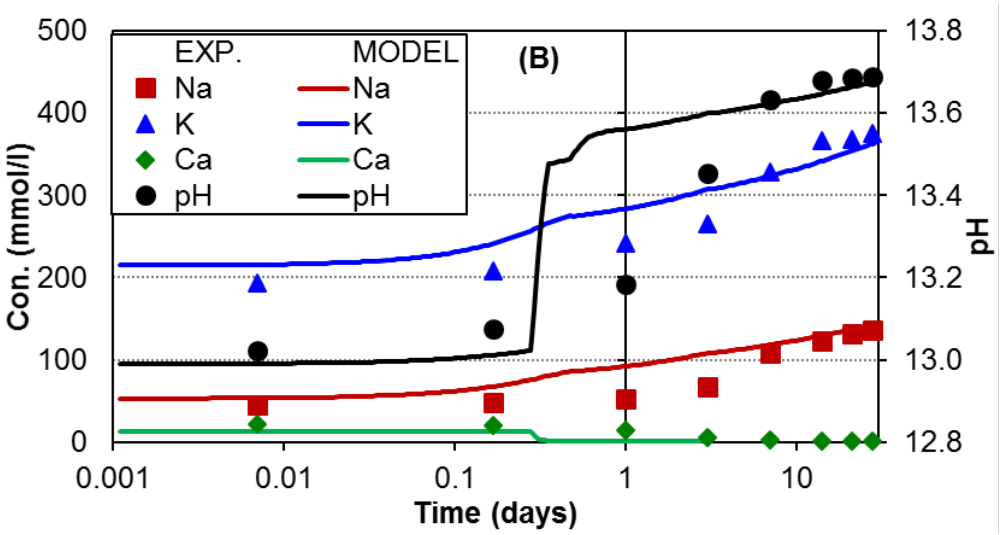

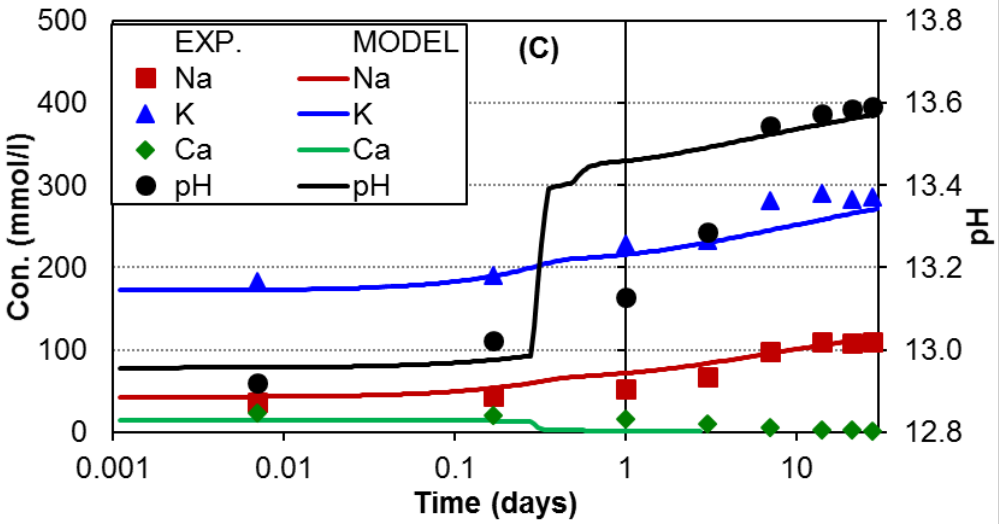

Fig. 4 Comparison of simulated pore solution concentration changes with experimental data [25] for hydrating OPC with w/c of (A) 0.4, (B) 0.45, and (C) 0.56

3.2. Slag cement system

3.2.1. Modelling approach

The coupled thermodynamic model described in **section 3.1.1**, including the solid solution model for C-S-H and C-A-S-H considered for the OPC system, with the same database and information relevant to cement hydration was also used to model the slag cement system. Thermodynamic calculations were performed for the dissolution of clinker minerals and the reaction of slag at every time step. The ions released as result of cement clinker dissolution and the reaction of the glass phase of slag determined the kind and amount of the formed phases and the composition of C-A-S-H. An equation to describe the degree of slag reaction was derived by fitting the various experimental data (**Fig. 5**) available in the literature [26-30], which included the reaction degree for the cement replacement by slag of 20–60% for up to 2 years of hydration, to a function. The influence of temperature, using the Arrhenius equation, and the surface area of the slag were included in the equation. The derived equation for the reaction degree of slag in percentage, α_{sg}, can be described as follows:

$$\alpha_{sg} = \left[A \times \ln(t) + B\right] \times S_{sg} \times \exp\left[-\frac{E_{Sg}}{R}\left(\frac{1}{T} - \frac{1}{T_0}\right)\right] \quad (12)$$

where,

$$A = -0.16 \times r_{sg} + 12.81 \quad (13)$$

$$B = 0.33 \times r_{sg} + 4.30 \quad (14)$$

$$S_{sg} = \frac{SA_{sg}}{4000} \quad (15)$$

$$E_{sg} = 400 \times r_{sg} + 32200 \quad (16)$$

where r_{sg} is the replacement ratio of slag (%), SA_{sg} is the Blaine value of slag (cm^2/g), and E_{sg} is the

activation energy of slag (J/mol), which was calculated from an equation given in ref. [31].

A distribution ratio of 0.45 mL/g is used for both Na^+ and K^+ uptake by C-A-S-H gel in the cement blended with slag system in order to predict ionic concentration in the pore solution.

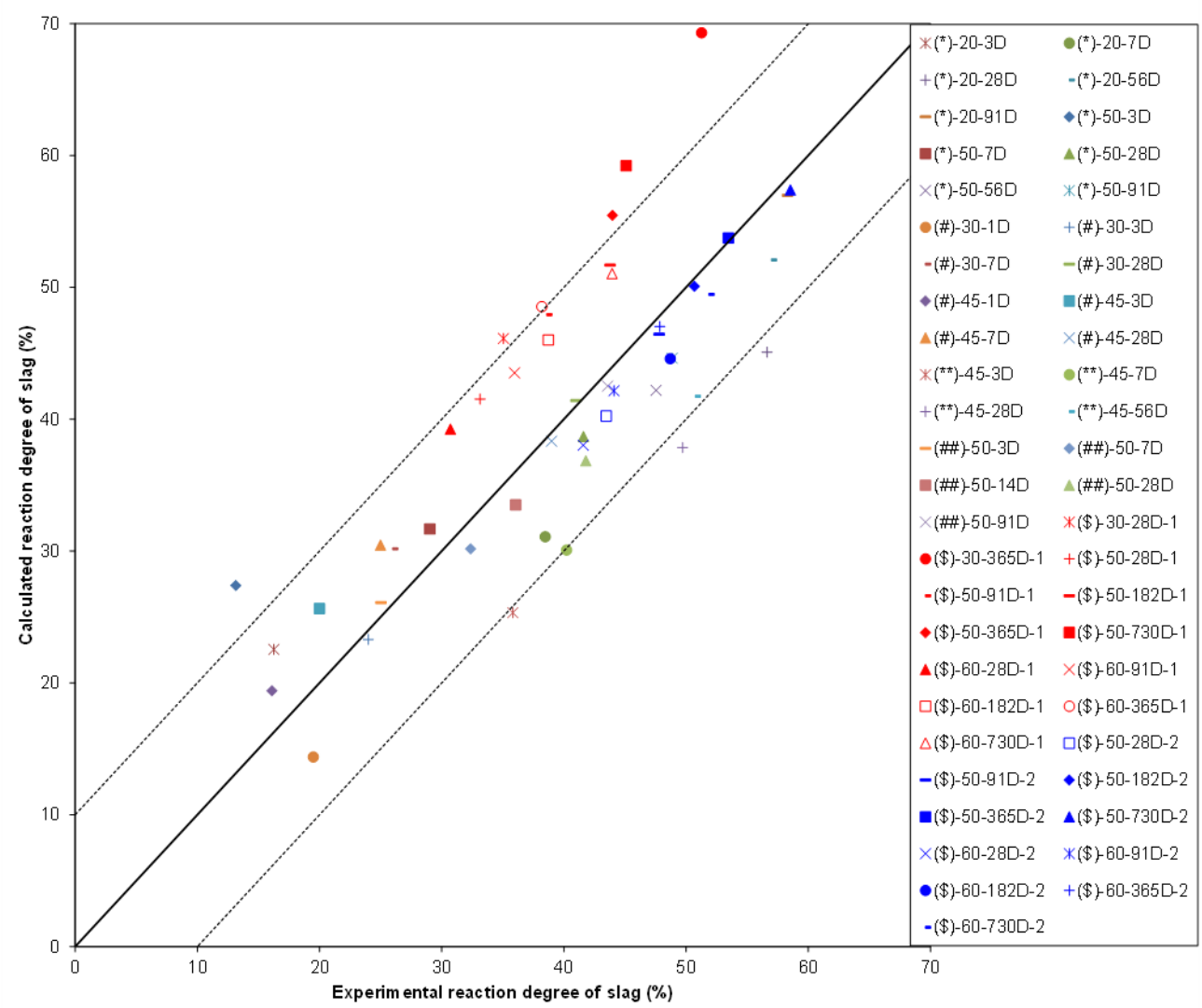

Fig. 5. Comparison of calculated reaction degree of slag using Eq. (12) with published ($[26], ##[27], **[28], *[29], and #[30]) experimental data. The dotted lines show ±10% deviation from y = x line. Notation: ( )-xx-yD: Reference-slag replacement ratio-curing period in days. Two types of slag in ref. (Lumley *et al.*, 1996) are used.

3.2.2. Simulation results and experimental data verification

315 The calculated composition of hydrates and the remaining un-reacted slag and clinker of the slag
316 cement system, which consists of 60% OPC and 40% slag, as a function of hydration time are
317 shown in **Fig. 6**(A) for the input parameters given in **Table 3** and the composition of slag tabulated
318 in **Table 4**. The predicted monocarboaluminate, which is formed through the dissolution of calcite,
319 is completely changed to hemicarboaluminate after approximately 7 days of hydration, thus
320 destabilising ettringite. The hydrated slag cement, with a degree of slag reaction of more than 70%,
321 has C-A-S-H solid solution, monosulfoaluminate, hydrotalcite, and monocarboaluminate, in
322 addition to decreasing trend of portlandite and ettringite as the main hydration products. The
323 calculated Ca/Si and Al/Si ratios of C-A-S-H as a function of hydration time are shown in **Fig. 6**(B).

324 **Table 4** Mineral composition of slag and chemical composition of glass in the slag

Mineral composition (wt. %)		*Glass composition (wt. %)*	
-Anhydrite	3.1	-SiO_2	30.80
-Glass	96.9	-Al_2O_3	13.80
Total	100.0	-Fe_2O_3	0.29
		-CaO	44.00
		-MgO	6.00
		-SO_3	3.45
		-Na_2O	0.23
		-K_2O	0.28
		Total	98.85

325

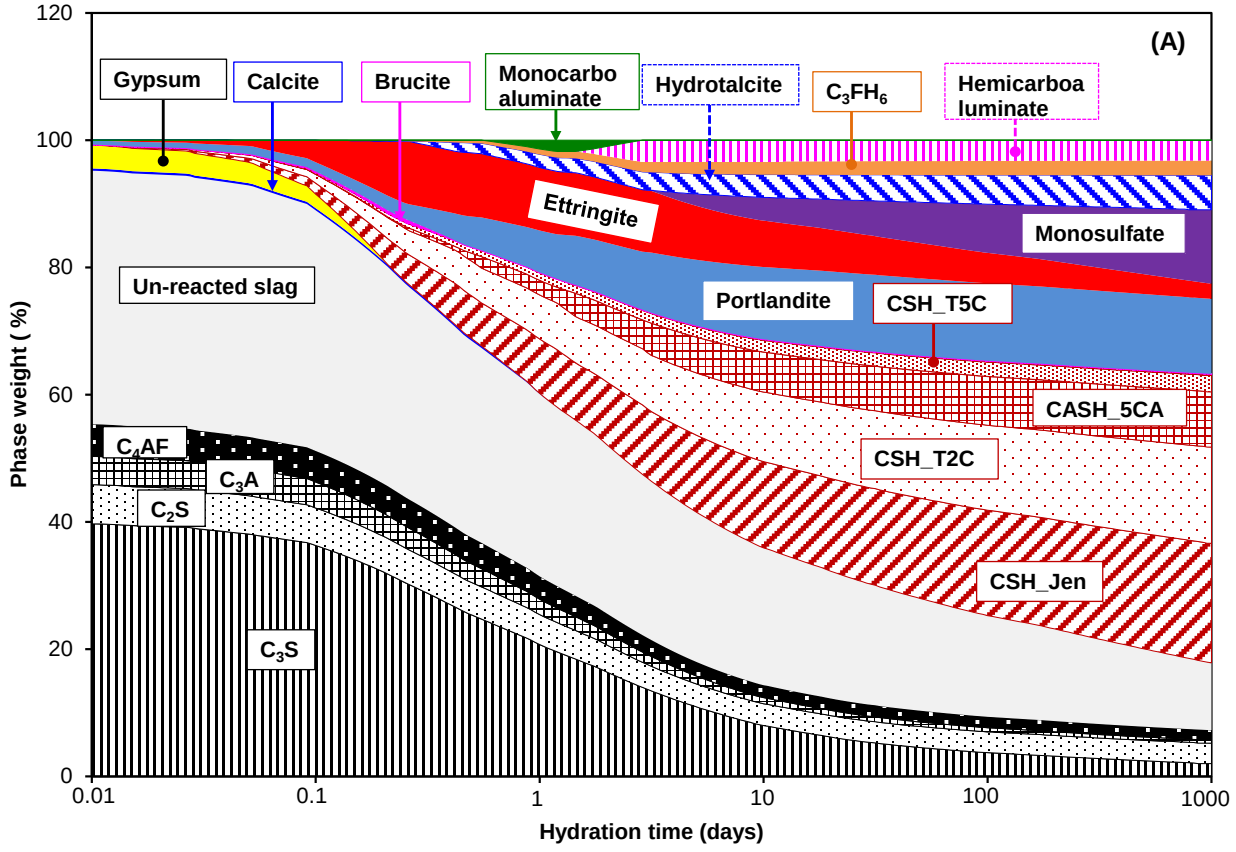

326

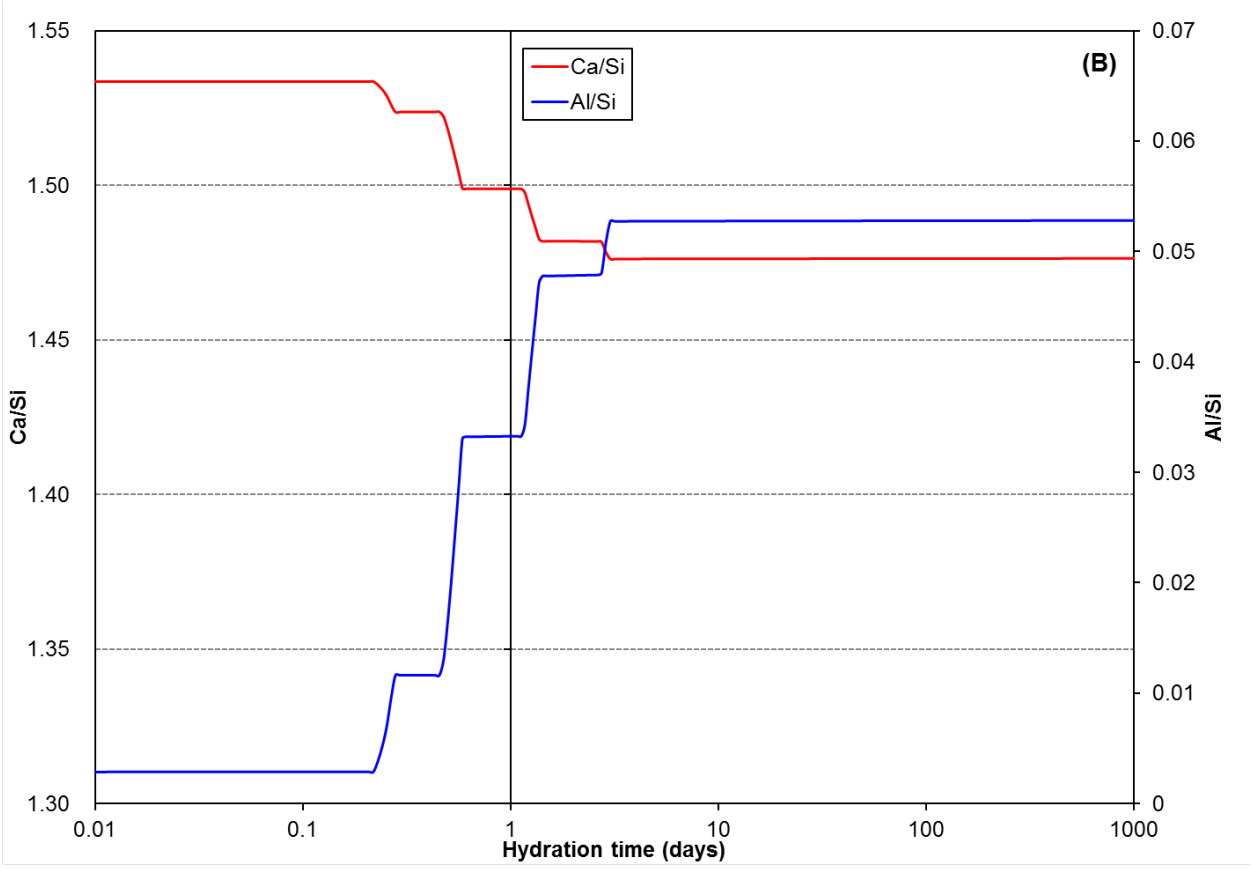

327

328 **Fig. 6.** Simulated phase (A), Ca/Si and Al/Si ratios of C-A-S-H (B) changes as a function of

329 hydration time for cement blended with slag (OPC: slag = 60:40)

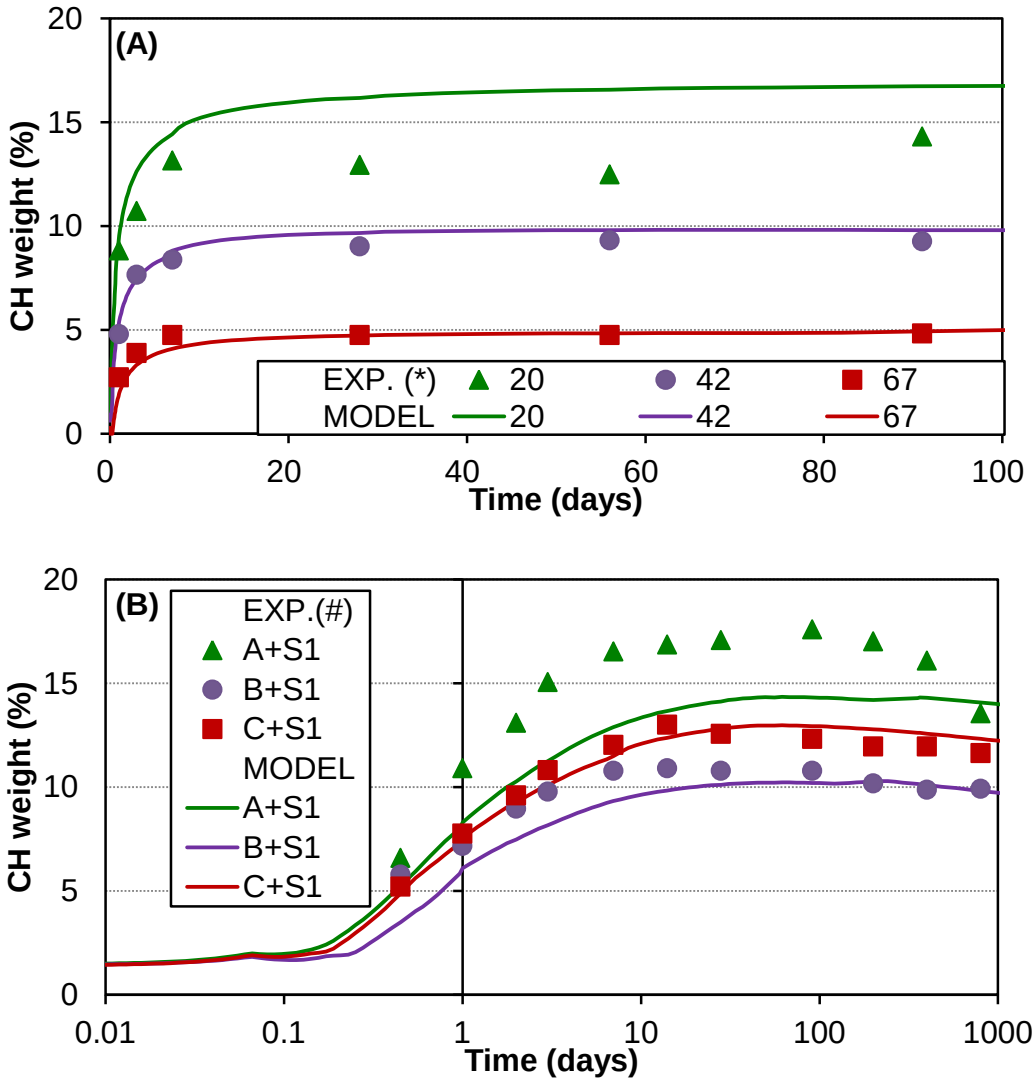

Fig. 7. Comparison of simulated portlandite changes with experimental data (*[32] and #[33]) for (A) various slag replacement ratios and (B) a constant replacement of 40% slag with various types of Portland cement as a function of hydration time for cement blended with slag

Fig. 7 compares the portlandite weight percentage predicted by the model and that determined by experiments [32-33] as a function of hydration time. The influence of the slag replacement ratio on the consumption of portlandite is shown in **Fig. 7**(A) while the effect of the chemical composition of Portland cement on the portlandite formation of the slag cement system is given in **Fig. 7**(B). The same composition of cement and slag and the mixing conditions as those given in ref. [32-33] were adopted in the simulation. In addition to a consistent trend between the predicted and measured values, the calculated portlandite content agrees very well with experimental results except for a

mixture containing 20% slag (20 in **Fig. 7** (A)) and white cement blended with slag (A+S1 in **Fig. 7**(B)). The portlandite has not completely consumed by slag hydration, even for a high replacement of slag and a long hydration time.

The main hydrates of the slag-blended cement (OPC:slag = 60:40) and slag and limestone-blended cement (OPC:slag:LS = 57.7:38.5:3.8) were predicted using the same details as those used in the experiment [34] as input, and the results are compared to XRD/Rietveld data in **Fig. 8** and **Fig. 9** respectively. The calculated phase changes show the same tendency as the measured data. The predicted portlandite, ettringite, monosulfoaluminate, monocarboaluminate, calcite, and un-reacted slag weight percentage show good agreement with experimental values, but the model slightly underestimates the amount of C-S-H/C-A-S-H in the hydrating slag-blended cement. Further, both the XRD results and the model predictions agree on the absence of monosulfoaluminate in the hydrated slag and limestone-blended cement, whereas the experimental results show the presence of hemicarboaluminate in the hydrates but the model did not predict it (**Fig. 9**). The element concentration predicted in the pore solution of the hydrating slag-blended cement is compared with experimentally determined values [35-36] in **Fig. 10**. The predicted dominant elements in the pore solution are consistent with experimental observations, and also the model predicts well the decrease of alkali concentration in the pore solution with increasing slag proportions as observed in the experiment.

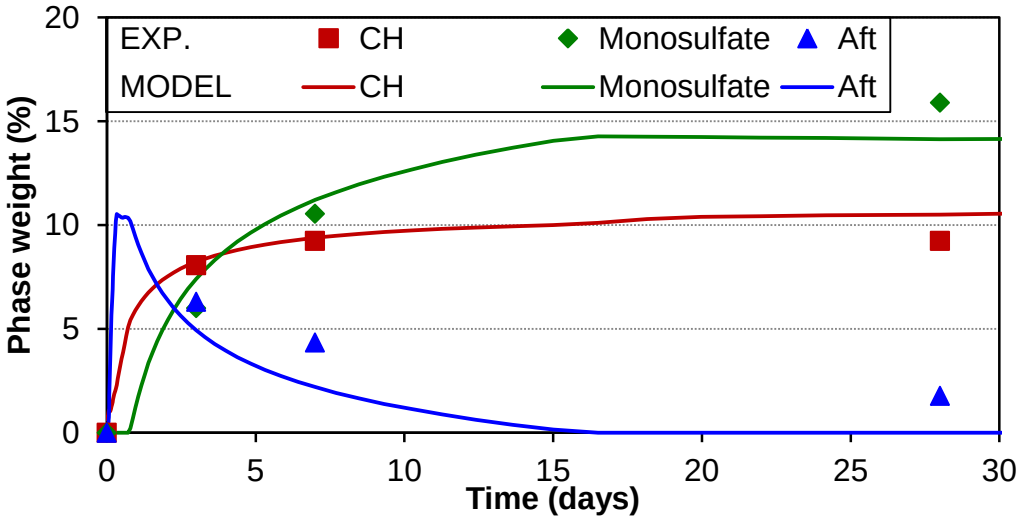

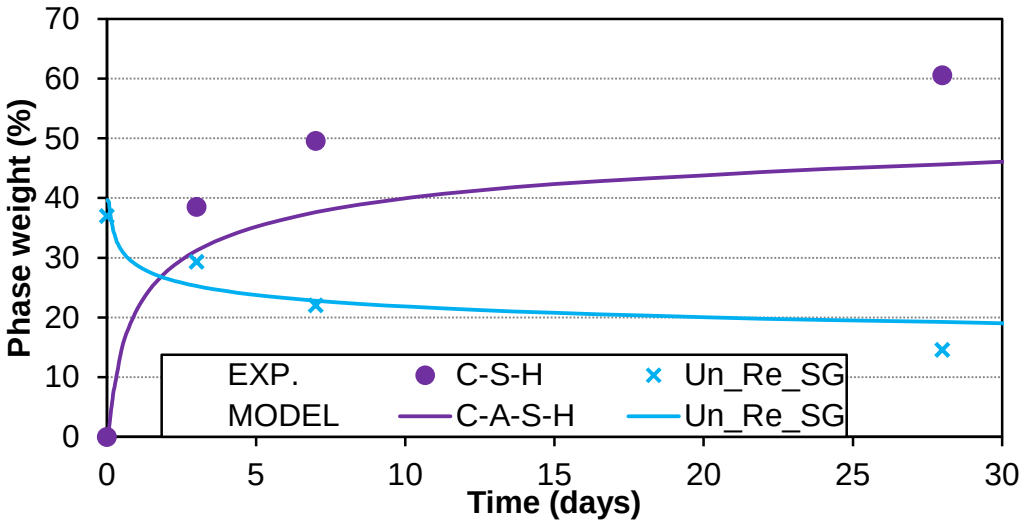

Fig. 8. Comparison of simulated portlandite (CH), monosulfate, ettringite (Aft), C-S-H/C-A-S-H and un-reacted slag (Un_Re_SG) changes with experimental data [34] as a function of hydration time for cement blended with slag (OPC: slag = 60:40)

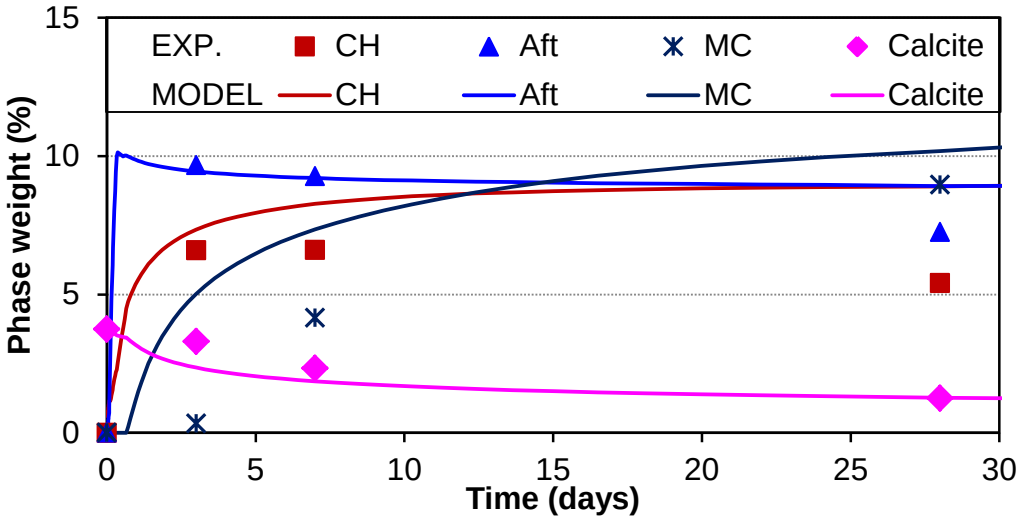

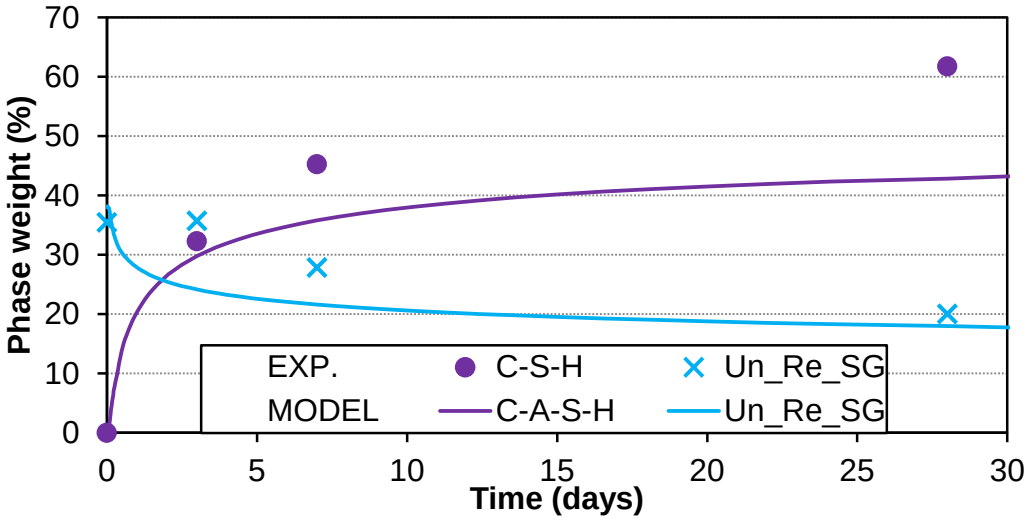

Fig. 9. Comparison of simulated portlandite (CH), ettringite (Aft), monocarboaluminate (MC), calcite, C-S-H/C-A-S-H and un-reacted slag (Un_Re_SG) changes with experimental data [34] as a function of hydration time for cement blended with slag and limestone (OPC: slag: LS = 57.7: 38.5: 3.8)

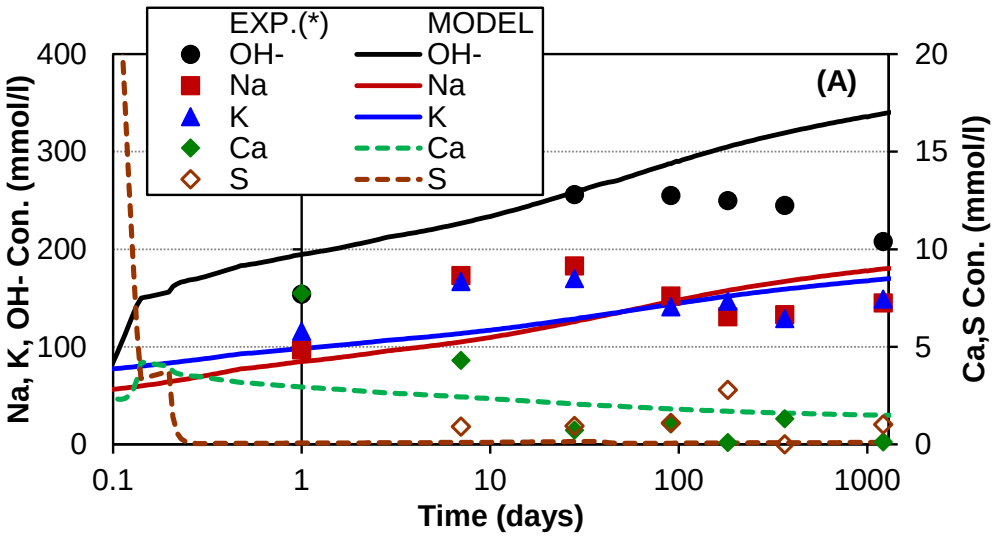

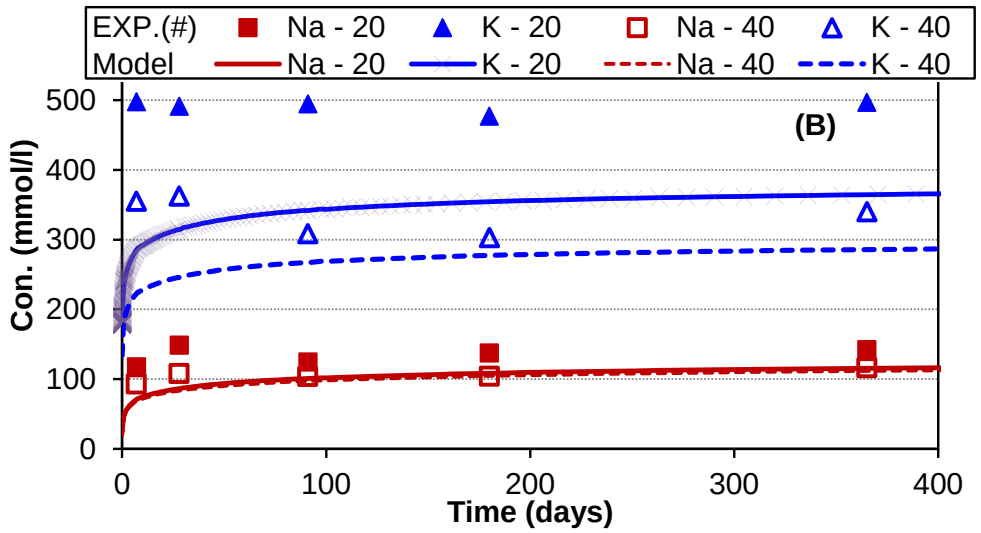

Fig. 10. Comparison of simulated pore solution/alkali concentration changes with experimental data (*[35]; #[36]) for (A) cement blended slag (OPC: slag = 50:50) and (B) cement containing 20% and 40% of slag

4. DISCUSSION

As demonstrated by the agreement between the experimental data and simulations results in slag cement systems, the approach used here can be applied to predict the compositions of the hydrate assemblage and pore solution. It should be noted that most of the slags used as supplementary cementitious materials have rather similar chemical compositions and high amorphous content. Different experimental results [32-36], which did not consider in the deriving equation (Eq. (12)) for slag reaction, have used to verify the hydration in slag-blended cement systems (**Fig. 7**–**Fig. 10**). This suggests a wider applicable range for the derived equation. However, the suitability of using this derived equation for a high replacement of cement by slag needs to be assessed because the equation was obtained for replacement levels of up to 60% slag.

The calculated results show the same kind of hydration products, such as C-A-S-H, portlandite, ettringite, hydrotalcite, and AFm phases, as observed in the experiments for hydrating Portland cement and cement blended with slag. Furthermore, the predicted quantities of the phases agree

well with the experimental values. The predicted Ca/Si and Al/Si ratios of C-A-S-H in hydrated OPC and slag-blended cements are compared with experimental data in **Table 5**. The distribution among four end-members of the initially selected six end-members determines the Ca/Si ratio of C-A-S-H, and the fraction of the CASH_5CA member controls the Al/Si ratio because the presence of the CASH_INFCA member is negligible. The consideration of low Ca/Si ratio of C-S-H as end-members of C-A-S-H solid solution in OPC decreases its Ca/Si ratio, whereas the low amount of CASH_5CA decreases the Al/Si ratio in slag-blended cement.

Table 5 Comparison between predicted and experimental Ca/Si and Al/Si ratios of C-A-S-H in hydrated OPC and blended cements. Experimental data from [*][2, 12, and 33] and [#][33]

	Ca/Si		Al/Si		Time
	Experimental	Predicted	Experimental	Predicted	(days)
OPC[*]	≈ 1.80	1.48	≈ 0.05	0.05	400
OPC: slag = 60:40[#]	≈ 1.55	1.47	≈ 0.15	0.06	400

A series of simulations were performed to evaluate the significance of the C-A-S-H solid solution in terms of precisely predicting the hydration products. The simulated portlandite weight percentage in the OPC and slag-blended cement was compared with experimental measurements in **Fig. 11** as an example. The simulation results for the case with six end-members of the C-A-S-H solid solution are shown in **Fig. 11**(A), along with the results of four end-members (without CASH_INFCA and CSH_TobH). The predicted results using four end-members of the solid solution match exactly with those using six end-members because the fractions of CASH_INFCA and CSH_TobH are insignificant (**Fig. 1**(A) and **Fig. 6**(A)). Both the predicted and the measured results are very close to the $y = x$ line for the OPC and blended cement, indicating the importance of six or four end-members of the C-A-S-H solid solution.

In contrast, another simulation was performed in which phase-equilibrium model with only CSH_Jen was assumed for C-S-H instead of the C-A-S-H solid solution model (**Fig. 11**(B)). The

modelled results are consistent with the experimental values for OPC, as observed in the case of the solid solution, which suggests that either a C-A-S-H solid solution or a CSH_Jen phase-equilibrium model can be used. However, poor agreement was found for the OPC containing slag, where incorporation of the CSH_Jen phase-equilibrium model underestimated the portlandite content in the blended cement. Therefore, it is important to consider the C-A-S-H solid solution model in order to predict precisely the hydration products in the blended cement. Despite some discrepancies in the Ca/Si or Al/Si ratio of C-A-S-H, the C-A-S-H solid solution model is more suitable for predicting the hydration products of both OPC and slag-blended cement. Future research on the thermodynamic models and laboratory experiments on C-A-S-H and the inclusion of other phases as end-members would enable us to predict Ca/Si and Al/Si ratios in the blended cements more accurately.

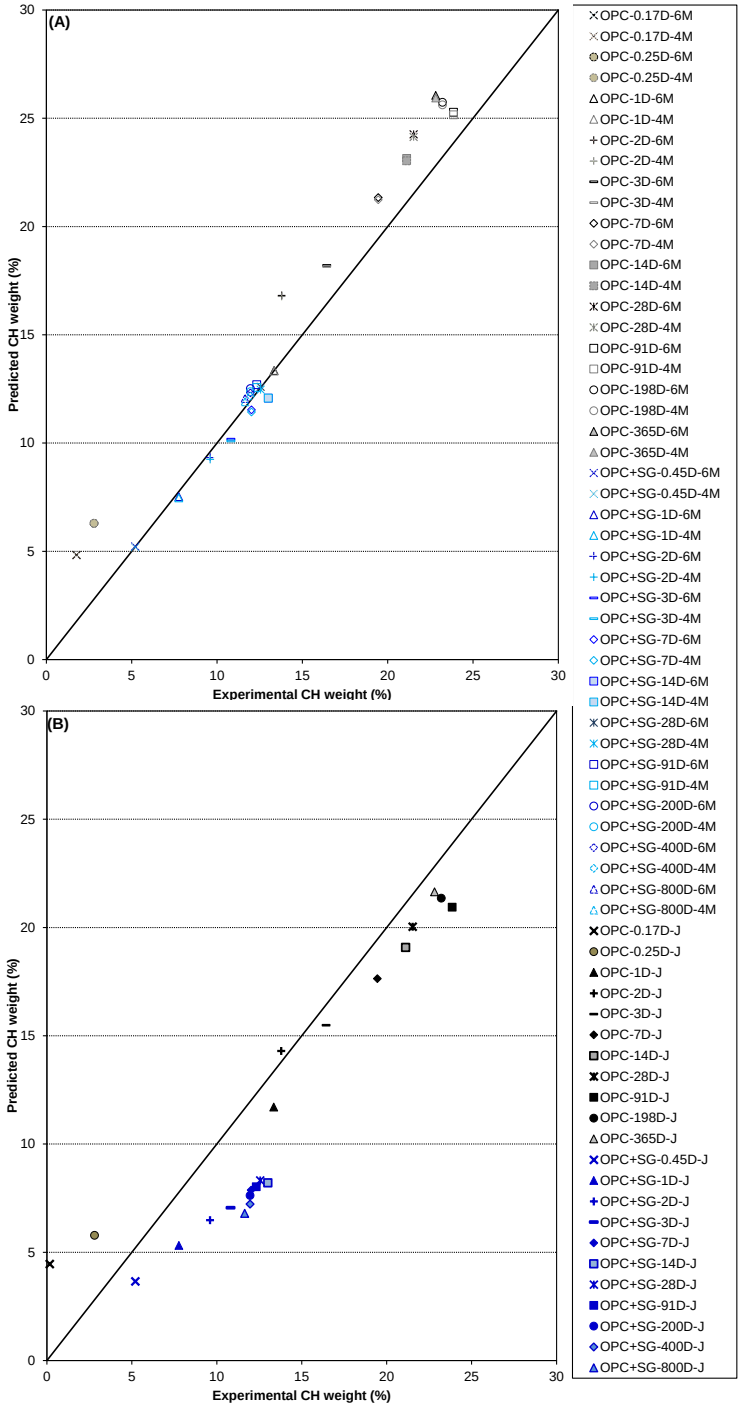

Fig. 11. Comparison of predicted portlandite weight percentage with experimental data [9 and 33] considering (A) C-A-S-H solid solution model and (B) without C-A-S-H solid solution model, but considered only the CSH_Jen phase for C-S-H. Notation: AA-xD-6M/4M/J: Binder-curing period in days-six end-members (CSH_Jen, CSH_T2C, CASH_5CA, CSH_T5C, CASH_INFCA and CSH_TobH) or four end-members (CSH_Jen, CSH_T2C, CASH_5CA, and CSH_T5C) solid solution for C-A-S-H or considered only the CSH_Jen phase.

5. CONCLUSIONS

The composition of the hydrate assemblage and pore solution chemistry of OPC and slag-blended cement as a function of hydration time were predicted using the PHREEQC integrated with empirical expressions for the dissolution of clinker minerals and reactions of slag. The main hydration products, such as C-A-S-H, portlandite, ettringite, hydrotalcite, and AFm phases, and major elements in the pore solution, such as Na, K, OH, Ca, S, Al, and Si, were predicted for the input of the chemical compositions of OPC and slag and mixing conditions. The considered solid solution model for C-A-S-H explains the varying Ca/Si and Al/Si ratios due to hydration and the addition of slag. The predicted results were verified with experimental data reported in the literature. The types of phases in the model predictions for hydrating Portland cement, cement blended with slag, and blended cement containing limestone were consistent with the experimental observations, and both the calculated and measured quantities showed good agreement. The predicted elements and the concentrations in the pore solution agreed well with the experimental results, but a proper model for the uptake of alkalis by C-A-S-H is necessary for better predictions in slag-blended cements. Comparing the simulated results considering the C-A-S-H solid solution model or not with experimental data for portlandite as an example emphasised the significance of the solid solution model in predicting the hydration products in slag-blended cement.

REFERENCES

1. M. S. Imbabi, C. Carrigan, S. McKenna, Trends and development in green cement and concrete technology, International Journal of Sustainable Built Environment 1 (2012) 194–216.
2. B. Lothenbach, K. Scrivener, R.D. Hooton, Supplementary cementitious materials, Cem. Concr. Res. 41 (2011) 1244–1256.
3. S. Miyahara *et al.* Durability and applications of environmental-friendly concrete with slag

and calcium activator, *5th International Conference on Construction Materials (ConMat'15*), (2015).

4. D. Rothstein, J. J. Thomas, B. J. Christensen, H. M. Jennings, Solubility of Ca-, S-, Al-, and Si-bearing solid phases in Portland cement pore solutions as a function of hydration time, Cem. Concr. Res. 32 (2002) 1663–1671.
5. A. Gruskovnjak et al., Hydration mechanism of super sulphated slag cement, Cem. Concr. Res. 38 (2008) 983–992.
6. R. Loser, B. Lothenbach, A. Leemann, M. Tuchschmid, Chloride resistance of concrete and its binding capacity - comparison between experimental results and thermodynamic modeling, Cement & Concrete Composites 32 (2010) 34–42.
7. B. Lothenbach, F. Winnefeld, Thermodynamic modelling of the hydration of Portland cement, Cem. Concr. Res. 36 (2006) 209–226.
8. B. Lothenbach, E. Wieland, A thermodynamic approach to the hydration of sulphate-resisting Portland cement, Waste Management 26 (2006) 706–719.
9. B. Lothenbach, G. Le Saout, E. Gallucci, K. Scrivener, Influence of limestone on the hydration of Portland cements, Cem. Concr. Res. 38 (2008) 848–860.
10. B. Lothenbach et al., Thermodynamic modelling of the effect of temperature on the hydration and porosity of Portland cement, Cem. Concr. Res. 38 (2008) 1–18.
11. B. Lothenbach et al., Sulfate ingress in Portland cement, Cem. Concr. Res. 40 (2010) 1211–1225.
12. K. De Weerdt et al., Hydration mechanisms of ternary Portland cements containing limestone powder and fly ash, Cem. Concr. Res. 40 (2011) 279–291.
13. Y. Elakneswaran and T. Ishida, Development and verification of an integrated physicochemical and geochemical modelling framework for performance assessment of cement-based materials, Journal of Advanced Concrete Technology, 12, (2014), 111–126.
14. B. Kolani et al., Hydration of slag-blended cements, Cement & Concrete Composites 34 (2012)

494 1009–1018.
495 15. R. J. Myers, S. A. Bernal, J. L. Provis, A thermodynamic model for C-(N-)A-S-H gel:
496 CNASH_ss. Derivation and validation, Cem. Concr. Res. 66 (2014) 27–47.
497 16. I. G. Richardson and G. W. Groves, Microstructure and microanalysis of hardened cement
498 pastes involving ground granulated blast-furnace slag, J Mater Sci., 27, (1992), 6204–6212.
499 17. C. A. J. Appelo, D. Postma, Geochemistry, groundwater and pollution: CRC Press Taylor &
500 Francis Group, 2009.
501 18. D. L. Parkhust, C. A. J. Appelo, A computer program for speciation, batch-reaction,
502 one-dimensional transport and inverse geochemical calculations, USGS report 1999.
503 19. K.S. Pitzer, Ion interaction approach: theory and data correlation, in: K.S. Pitzer (Ed.), Activity
504 Coefficients in Electrolyte Solutions, CRC Press, Boca Raton, 1991, pp. 75–153.
505 20. D.A. Kulik, Improving the structural consistency of C-S-H solid solution thermodynamic
506 models, Cem. Concr. Res. 41 (2011) 477–495.
507 21. L. J. Parrot, D. C. Killoh, Prediction of cement hydration, British Ceramic Proceedings 35
508 (1984) 41–53.
509 22. S. R. Charlton, D. L. Parkhurst, Modules based on the geochemical model PHREEQC for use in
510 scripting and programming languages, Computers & Geosciences 37 (2011) 1653–1663.
511 23. W. Chen and H. J. H. Brouwers, Alkali binding in hydrated Portland cement paste, Cement and
512 Concrete Research, 40, (2010), 716–722.
513 24. T. Matschei, B. Lothenbach, F.P. Glasser, The AFm phase in Portland cement, Cem. Concr. Res.
514 37 (2007) 118–130.
515 25. L.A Larbi, et al, The chemistry of pore fluid of silica fume-blended cement systems, Cement
516 and Concrete Research, 20, (1990), 506-516.
517 26. J. S. Lumley, R. S. Gollop, G. K. Moir, H. F. W. Taylor, Degrees of reaction of the slag in some
518 blends with Portland cements, Cem. Concr. Res. 26 (1996)139–51.
519 27. T. Sagawa, T. Nawa, Hydration of blast furnace slag cement and effect of water to cement ration

on hydration of blast furnace slag cement, Cement Science and Concrete Technology 60 (2006) 82–87. (In Japanese)

28. T. Sagawa, T. Ishida, Y. Luan, T. Nawa, Hydrate composition analysis and micro structure characteristics of Portland cement-blast furnace slag system, Journal of JSCE E 66 (2010) 311–324. (In Japanese)
29. E. Sakai, H. Imoto, M. Daimon, Hydration and strength development of blast furnace slag cement, Proceedings of JCI 26 (2004) 135–140. (In Japanese)
30. N. Takamatsu, I. Maruyama, Study on volume deformation and hydration degree of blast furnace slag replaced matrix, Proceedings of JCI 31 (2009) 187–192. (In Japanese)
31. S.J. Barnett, M.N. Soutsos, S.G. Millard, J.H. Bungey, Strength development of mortars containing ground granulated blast-furnace slag: Effect of curing temperature and determination of apparent activation energies, Cem. Concr. Res. 36 (2006)434–440.
32. T. Iyoda, Y. Dan, The effect of temperature on hydration rate of slag in blended cement, Proceeding of JSCE 333 committee symposium (2007) II59–62. (In Japanese)
33. V. Kocaba, Development and evaluation of methods to follow microstructural development of cementitious systems including slags, PhD thesis, ÉCOLE POLYTECHNIQUE FÉDÉRALE DE LAUSANNE, 2009.
34. S. Hoshino, K. Yamada, H. Hirao, XRD/Rietveld analysis of the hydration and strength development of slag and limestone blended cement, Journal of Advanced Concrete Technology 4 (2006) 357–367.
35. T. Maruya, Y. Matsuoka, Durability assessment of binders by analysing liquid and solid phase, JSCE 478 (1993) 41–50 (In Japanese)
36. E. Schafer, “Einfluss der Reaktionen verschiedener Zementbestandteile auf den alkalihaushalt der Porenlösung des Zementsteins”, *PhD thesis*, Clausthal University of Technology, Clausthal-Zellerfeld, Germany, (2004).